ChemComm

COMMUNICATION

View Article Online
View Journal | View Issue

Cite this: *Chem. Commun.*, 2016, 52, 5946

Received 23rd March 2016,
Accepted 29th March 2016

DOI: 10.1039/c6cc02513g

www.rsc.org/chemcomm

Co/CoO nanoparticles immobilized on Co–N-doped carbon as trifunctional electrocatalysts for oxygen reduction, oxygen evolution and hydrogen evolution reactions†

Xian Zhang,[ab] Rongrong Liu,[ab] Yipeng Zang,[ab] Guoqiang Liu,[ab] Guozhong Wang,[a] Yunxia Zhang,[a] Haimin Zhang*[a] and Huijun Zhao[ac]

Co/CoO nanoparticles immobilized on Co–N-doped carbon were successfully developed using shrimp-shell derived N-doped carbon nanodots as precursors by a combined approach of polymerization and pyrolysis, as electrocatalysts exhibiting trifunctional catalytic activities toward oxygen reduction, oxygen evolution and hydrogen evolution reactions and high performance in rechargeable zinc–air batteries.

Electrocatalysts for oxygen reduction reaction (ORR), oxygen evolution reaction (OER) and hydrogen evolution reaction (HER) are of particular significance for some promising clean energy technologies such as metal–air batteries, fuel cells and water splitting to generate hydrogen and oxygen.[1] Moreover, effective rechargeable metal–air batteries and fuel cells require bifunctional catalysts with low overpotentials for both OER and ORR.[1,2] Bifunctional electrocatalysts for the OER and HER together in the same electrolyte are of practical values to accomplish the overall water splitting.[2] However, current Pt-based electrocatalysts and iridium/ruthenium oxide electrocatalysts cannot meet the practical requirements of these energy devices owing to their non-bifunctional ORR/OER or OER/HER activity and high cost/source scarcity.[3] Therefore, development of multifunctional electrocatalysts with high activity and low cost remains a great challenge for the practical applications of related energy technologies.

Up to now, various cobalt-based materials have been reported for HER, such as metal Co, CoS_2, CoP, and CoSe, showing high catalytic activities.[4] Recently, cobalt oxides/(oxy)hydroxides have demonstrated better catalytic activities toward OER.[5] This means that cobalt-based materials with different cobalt active species are capable of accomplishing the overall water splitting to produce hydrogen and oxygen.[2,5b,6] However, the metal Co or Co_xO_y material possesses many disadvantages, such as easy accumulation and low conductivity, which would decrease the catalytically active sites and hamper the transport of electrons or protons during the electrocatalysis.[7] It is noteworthy that recently the cobalt/carbon based electrocatalysts have demonstrated bifunctional electrocatalytic activities, such as N-CG–CoO and $Co_{1-x}Fe_xS$@N-MC for ORR/OER;[8] CoO_x@CN and CoMnO@CN for OER/HER.[9] The introduction of graphitic carbon not only improves the electron transfer and mass transport during the electrocatalysis, but also the Co–N_x moieties formed in the graphitic carbon structure provide catalytically active sites for high ORR performance.[4d,10b] Based on the above discussion, development of carbon-based electrocatalysts with cobalt active species such as metal Co, cobalt oxides and Co doping may realize the multifunctionality of ORR, OER and HER.

Herein, we report the synthesis of Co/CoO nanoparticles immobilized on Co–N-doped carbon (Co/CoO@Co–N-C) using shrimp-shell derived N-doped carbon nanodots (N-CNs) as carbon and nitrogen sources by a combined approach of polymerization and pyrolysis. Fig. 1 shows a schematic illustration of the synthesis of Co/CoO@Co–N-C catalysts (see the Experimental section for detailed information, ESI†). The experimental results demonstrate that Co/CoO@Co–N-C obtained by pyrolysis at 800 °C (Co/CoO@Co–N-C-800) exhibits a microporous structure and a high surface area of 647.7 $m^2\ g^{-1}$. As an electrocatalyst, Co/CoO@Co–N-C-800 displays superior trifunctional ORR, OER and HER catalytic activities in alkaline media. Furthermore, Co/CoO@Co–N-C-800

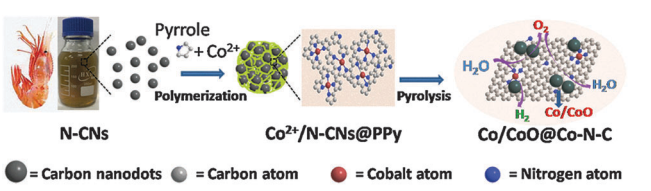

Fig. 1 Schematic illustration of the synthesis of Co/CoO@Co–N-C.

[a] *Key Laboratory of Materials Physics, Centre for Environmental, Energy Nanomaterials, Anhui Key Laboratory of Nanomaterials, Nanotechnology, Institute of Solid State Physics, Chinese Academy of Sciences, Hefei 230031, China. E-mail: zhanghm@issp.ac.cn*

[b] *University of Science and Technology of China, Hefei 230026, China*

[c] *Centre for Clean Environment and Energy, Griffith University, Gold Coast Campus, QLD 4222, Australia*

† Electronic supplementary information (ESI) available: Details of experiments, supporting SEM and TEM images, XPS analysis and electrochemical measurements. See DOI: 10.1039/c6cc02513g

was evaluated as an air cathode material for rechargeable zinc–air battery measurements, exhibiting high performance and recycling stability.

Our previous work has demonstrated that shrimp-shell derived carbon nanodots possess small nanodot sizes (1.5–5.5 nm) and surface rich N- and O-containing functional groups, favorable for further assembling and transforming into N-doped graphitic carbon for ORR (Fig. S1, ESI†).[11] In this work, shrimp-shell derived N-CNs were used as carbon and nitrogen sources to fabricate cobalt-based N-doped carbon materials for multifunctional electrocatalysis. After polymerization, a Co^{2+} containing composite exhibits particle-like aggregates (Fig. S2a, ESI†), and a similar morphology can be observed for a pyrolytic sample (Fig. S2b, ESI†, take Co/CoO@Co–N-C-800 as an example). Fig. 2a shows the XRD patterns of pyrolytic samples obtained at different temperatures. As shown, all pyrolytic samples exhibit an interplane (002) diffraction peak at around 24.7°, ascribed to graphitic carbon.[12] Additionally, some new diffraction peaks due to the presence of CoO and metal Co can be observed for Co/CoO@Co–N-C-700 and Co/CoO@Co–N-C-800, while only metal Co can be found for the pyrolytic samples at 900 °C and 1000 °C (denoted as Co@Co–N-C-900 and Co@Co–N-C-1000), indicating that high temperatures are unfavourable for the formation of CoO owing to oxygen removal at such temperatures. The XRD results reveal that pyrolysis temperature plays an important role in determining the composition of the resulting sample, thus possibly leading to different electrocatalytic activities. Detailed structure information on pyrolytic samples (*e.g.*, Co/CoO@Co–N-C-800) was obtained by TEM characterization. As shown, a stacked carbon structure with deposited Co-related nanoparticles can be observed (Fig. 2b and Fig. S3, ESI†). The corresponding energy-filtered TEM (EFTEM) spectrum analysis (Fig. 2c) verifies that Co/CoO@Co–N-C-800 is composed of O, Co, N and C elements, indicating the possible presence of metal Co, cobalt oxide and doped N in the sample. From the elemental mapping signals of graphitic carbon without Co-related nanoparticles (Fig. S4, ESI†), we observe that Co and N elements are uniformly distributed in a graphitic carbon structure, implying that the Co atoms are possibly bonded with the doped N in the carbon structure to form Co–N_x moieties responsible for electrocatalytic activity.[10a,13,14a] Furthermore, the Co-related nanoparticles deposited onto graphitic carbon exhibit two sets of crystalline lattices of 0.246 nm and 0.207 nm, corresponding to the (111) plane of the CoO phase and the (111) plane of the Co phase, respectively, consistent with the XRD results of Co/CoO@Co–N-C-800 (Fig. 2d and Fig. S3c–e, ESI†). The above TEM analysis confirms that Co-related nanoparticles onto graphitic carbon are Co/CoO co-existent.

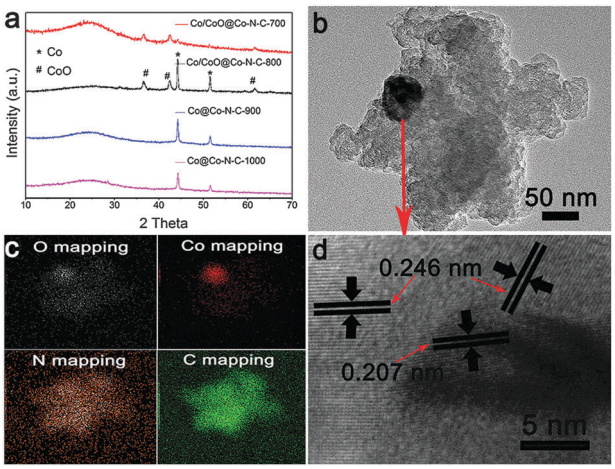

Fig. 2 (a) XRD patterns of the fabricated cobalt-based N-doped carbon materials obtained at different pyrolysis temperatures. (b) TEM image of Co/CoO@Co–N-C-800. (c) Energy-filtered TEM elemental mapping of Co/CoO@Co–N-C-800. (d) High resolution TEM image of an individual Co/CoO nanoparticle.

Fig. S5a (ESI†) shows surface survey XPS spectra of Co/CoO@Co–N-C-800, indicating the presence of C (83.41%), O (7.94%), N (7.44%) and Co (1.21%) elements. The high resolution N 1s spectrum (Fig. S5b, ESI†) can be divided into four peaks at 398.5, 400.2, 401.1, and 404.6 eV, corresponding to pyridinic-N (28.1%), pyrrolic-N (26.4%), graphitic-N (33.6%), and quaternary N^+–O^- (11.9%).[14] It has been generally accepted that pyridinic-N and pyrrolic-N can serve as metal-coordination sites owing to their lone-pair electrons, whereas pyridinic-N and graphitic-N are responsible for ORR.[14] In this work, pyrrole not only triggers a polymerization reaction, but also acts as an additional nitrogen source to enhance the nitrogen doping level, favourable for improving catalyst's electrocatalytic activity (Tables S1 and S2 in the ESI†).[14] The high resolution Co 2p spectrum (Fig. S5c, ESI†) shows five peaks at 778.5, 780.5, 786.1, 796.4 and 803.6 eV. Among them, the intense peaks at 786.1 and 803.6 eV were satellite peaks that can be ascribed to the shakeup excitation of the high-spin Co^{2+} ions.[3] The peaks at 778.5 and 780.5 eV can be ascribed to the binding energies of the $2p_{3/2}$ orbitals of Co species and the peak at 796.4 eV corresponds to the $2p_{1/2}$ orbitals of Co species.[10a] After deconvolution, the peak at around 780.5 eV is assigned to the CoO_x phase, while that at around 778.5 eV corresponds to the Co^0 phase.[10a] The XPS analysis is consistent with the XRD results. As shown in Fig. S6 (ESI†), the Brunauer–Emmett–Teller surface area and total pore volume of Co/CoO@Co–N-C-800 are 647.7 $m^2\ g^{-1}$ and 0.342 $cm^3\ g^{-1}$, respectively, indicating a microporous structure with high surface area and large pore volume, favorable for the exposure of catalytically active sites and electrocatalysis-related mass transport.

As an electrocatalyst, we first evaluated the ORR performance of Co/CoO@Co–N-C-800 in 0.1 M KOH solution. The cyclic voltammetry (CV) curve indicates that Co/CoO@Co–N-C-800 possesses comparable catalytic activity for ORR to that of Pt/C (Fig. S7, ESI†). Fig. 3a shows the linear sweep voltammogram (LSV) responses of pyrolytic samples and Pt/C. As shown, the investigated electrocatalysts exhibit the onset potentials (and half-wave potentials) of −0.08 (−0.23), −0.05 (−0.17), −0.09 (−0.22), −0.11 (−0.23) and −0.03 (−0.16) V for Co/CoO@Co–N-C-700, Co/CoO@Co–N-C-800, Co@Co–N-C-900, Co@Co–N-C-1000 and Pt/C, respectively. Very approximate onset and half-wave potential values of Co/CoO@Co–N-C-800 and Pt/C indicate a superior ORR activity of Co/CoO@Co–N-C-800. The ORR performances of comparative samples (N-CN-800, PPy/N-CN-800,

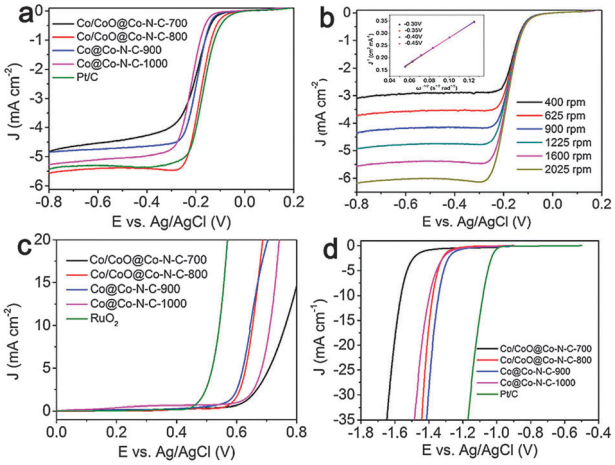

Fig. 3 (a) LSV curves of cobalt-based N-doped carbon materials and Pt/C in O_2-saturated 0.1 M KOH solution at a scan rate of 10 mV s^{-1} and a rotation speed of 1600 rpm. (b) LSV curves of Co/CoO@Co–N-C-800 at different rotation speeds and the inset showing the corresponding K–L plots. (c) LSV curves of cobalt-based N-doped carbon materials and RuO_2 in O_2-saturated 0.1 M KOH solution at a scan rate of 5.0 mV s^{-1}. (d) LSV curves of cobalt-based N-doped carbon materials and Pt/C in N_2-saturated 0.1 M KOH solution at a scan rate of 5.0 mV s^{-1}.

and Co-PPy-800) were also investigated in 0.1 M KOH solution (Fig. S8, ESI†). Apparently, the introduction of pyrrole and cobalt sources can significantly improve the ORR performance of catalysts owing to the improved N doping level resulting from pyrrole (Tables S1 and S2, ESI†) and Co-related active species creating more catalytic active sites.[10,13,14] Additionally, Co/CoO@Co–N-C-800 also displays the highest limiting current within the investigated potential range among all catalysts (Fig. 3a and Fig. S8 in the ESI†), further indicating its superior ORR performance. Compared to other Co-based catalysts, the high ORR catalytic activity of Co/CoO@Co–N-C-800 may be due to many attributes such as high surface area, porous structure and suitable content of ORR-related active species (*e.g.*, Co, N doping).[9a] Fig. 3b shows the LSV curves of Co/CoO@Co–N-C-800 obtained from an O_2-saturated 0.1 M KOH solution at different rotation rates. Based on Fig. 3b and the corresponding Koutecky–Levich (K–L) plots (inset in Fig. 3b), the average value of the number of transferred electrons at −0.30 to −0.45 V was calculated to be 3.8 for Co/CoO@Co–N-C-800, approximate to the theoretical value of the Pt/C catalyst (n = 4.0), indicating a near four electron ORR process. The resistance to fuel molecule interference and durability are important parameters to evaluate an ORR catalyst for practical application. Fig. S9 (ESI†) shows the crossover effect and durability measurements of Co/CoO@Co–N-C-800 and Pt/C catalysts under identical experimental conditions. Apparently, Co/CoO@Co–N-C-800 exhibits high resistance to the methanol crossover effect and good durability. This is very important for the practical application of the Co/CoO@Co–N-C-800 catalyst.

As we know, it is critically important to develop an electrocatalyst with bifunctional ORR and OER catalytic activity for a rechargeable zinc–air battery.[15] In this work, the OER activities of pyrolytic samples and commercial RuO_2 catalysts were investigated in 0.1 M KOH solution. Fig. 3c shows the polarization curves of all investigated catalysts. As shown, the measured potentials at a current density of 10 mA cm^{-2} are 0.76, 0.64, 0.63, 0.71 and 0.55 V for Co/CoO@Co–N-C-700, Co/CoO@Co–N-C-800, Co@Co–N-C-900, Co@Co–N-C-1000 and RuO_2, respectively, indicating that the samples obtained at 800 and 900 °C possess very similar OER catalytic activity. However, too low or too high pyrolysis temperature (*e.g.*, 700 or 1000 °C) is not beneficial for high OER activity of catalysts. We cannot provide direct evidence to confirm the origins of OER activity of these two catalysts. However, based on the aforementioned ORR measurements and material characterization results (XRD and XPS), the presence of metal Co in these two catalysts may be beneficial for improving the OER activity. With increasing pyrolysis temperature to 1000 °C, the decrease of N doping content (Table S1, ESI†) may reduce the synergistic effect of Co–N doping in graphitic carbon, thus resulting in decreased OER activity of Co@Co–N-C-1000. The durability test shows that a decrease in potential of only 0.08 V in the initial activity was observed at a current density of 10 mA cm^{-2} for Co/CoO@Co–N-C-800 after 1000th run, indicating a high applicable stability of Co/CoO@Co–N-C-800 (Fig. S10, ESI†). The above results indicate that Co/CoO@Co–N-C-800 possesses bifunctional catalytic activities for both ORR and OER. Furthermore, we also evaluated the HER performance of pyrolytic samples and commercial Pt/C in 0.1 M KOH solution. On the one hand, pairing the OER and HER catalysts together in the same electrolyte is of practical values to accomplish the overall water splitting. On the other hand, alkaline electrolysis is an attractive alternative to proton exchange membrane (PEM)-based electrolysis because the non-noble metal electrocatalysts involved in alkaline electrolysis tend to be more stable and exhibit relatively high activities for the HER.[4b,16] As shown in polarization curves of all investigated catalysts (Fig. 3d), the measured potentials at a current density of 20 mA cm^{-2} are −1.61, −1.40, −1.37, −1.44 and −1.12 V for Co/CoO@Co–N-C-700, Co/CoO@Co–N-C-800, Co@Co–N-C-900, Co@Co–N-C-1000 and Pt/C, respectively, confirming that Co/CoO@Co–N-C-800, Co@Co–N-C-900 and Co@Co–N-C-1000 possess very close HER catalytic activity, indicating that the increase of metal Co content in a carbon structure with pyrolysis temperature (Table S1, ESI†) may be favourable for improving the HER activity.[4a] Also, Co/CoO@Co–N-C-800 also demonstrates high durability during HER (Fig. S11, ESI†). Recently, carbon-based electrocatalysts with different formed cobalt active species have demonstrated high activities of ORR, OER and HER.[2,6,17] It is believed that the trifunctionality of ORR, OER and HER of Co/CoO@Co–N-C-800 in this work can be ascribed to a synergistic effect of Co, CoO and Co–N doping in a graphitic carbon structure creating catalytically active sites.

The primary zinc–air battery device was constructed by assembling a zinc foil anode with a Co/CoO@Co–N-C-800 loaded air cathode, and was tested in a 6.0 M KOH electrolyte. As shown in Fig. 4a the open-circuit voltage was determined to be ~1.4 V for Co/CoO@Co–N-C-800, almost identical to that

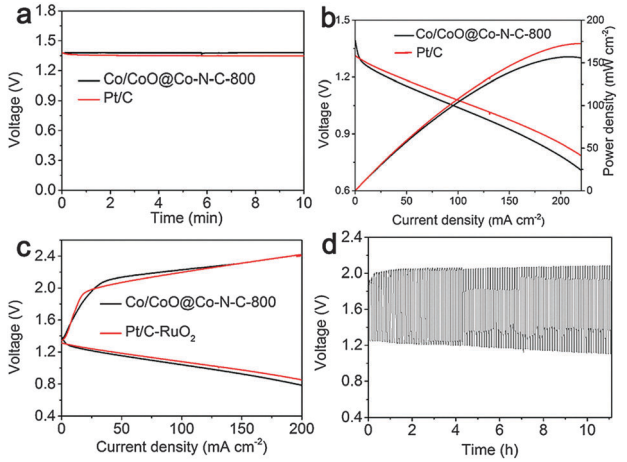

Fig. 4 (a) Open circuit voltage measurements of zinc–air batteries assembled with different catalysts. (b) Power density plots of zinc–air batteries assembled with different catalysts. (c) Charge–discharge polarization curves of rechargeable zinc–air batteries made from different catalysts. (d) Recycling durability test of a rechargeable zinc–air battery made from Co/CoO@Co–N-C-800.

of Pt/C. Fig. 4b shows the power density curves of zinc–air batteries assembled with Co/CoO@Co–N-C-800 and Pt/C. In the discharge process, the zinc–air battery made from Co/CoO@Co–N-C-800 shows a high current density of 96 mA cm^{-2} at 1.0 V, close to that of the Pt/C based zinc–air battery (113 mA cm^{-2} at 1.0 V) (Fig. 4b). The peak power density of the zinc–air battery assembled with Co/CoO@Co–N-C-800 is 157 mW cm^{-2} at 0.75 V, which is approximate to that of the Pt/C based zinc–air battery (173 mW cm^{-2} at 0.7 V). Based on its efficient ORR and OER performance, Co/CoO@Co–N-C-800 was further constructed to a rechargeable zinc–air battery, which was tested in a 6.0 M KOH electrolyte including 0.2 M zinc acetate. To obtain a meaningful comparison, a commercial mixture of Pt/C and RuO_2 with a mass ratio of 1 : 1 was used in this work for rechargeable battery measurements. During the charge–discharge process (Fig. 4c), the battery made from Co/CoO@Co–N-C-800 exhibits similar current densities to the rechargeable battery assembled with Pt/C–RuO_2, indicating the superior charge–discharge performance of Co/CoO@Co–N-C-800 in the rechargeable zinc–air battery. The durability test of Co/CoO@Co–N-C-800 is shown in Fig. 4d. The initial charge and discharge potentials of the Co@CoO/Co–N-C-800 based zinc–air battery are 1.92 and 1.25 V, respectively. After 100 cycles, the charge and discharge potentials were 2.05 and 1.19 V, respectively, indicating high recycling durability. Concurrently, as cathode and anode materials, Co/CoO@Co–N-C-800 was also loaded onto carbon fiber paper to evaluate water splitting to generate hydrogen and oxygen in 0.1 M KOH solution. As shown in Fig. S12 (ESI†), a number of air bubbles can be observed due to the generation of hydrogen and oxygen on the Co/CoO@Co–N-C-800 cathode and anode by water splitting, further confirming the superior OER and HER catalytic activity of Co/CoO@Co–N-C-800.

In summary, Co-based N-doped carbon materials were successfully fabricated using shrimp-shell derived N-doped carbon nanodots as precursors by a combined approach of polymerization and pyrolysis. As an electrocatalyst, Co/CoO@Co–N-C-800 exhibited trifunctional catalytic activities toward ORR, OER and HER, and high performance of a rechargeable zinc–air battery and water splitting.

This work was financially supported by the CAS Pioneer Hundred Talents Program, the Users with the Potential Program (2015HSC-UP006, Hefei Science Center, CAS), and the Natural Science Foundation of China (Grant No. 51372248 and 51432009).

Notes and references

1 (*a*) Y. Liang, Y. Li, H. Wang, J. Zhou, J. Wang, T. Regier and H. Dai, *Nat. Mater.*, 2011, **10**, 780; (*b*) Z. Peng, S. A. Freunberger, Y. Chen and P. G. Bruce, *Science*, 2012, **337**, 563.
2 Y.-P. Zhu, Y.-P. Liu, T.-Z. Ren and Z.-Y. Yuan, *Adv. Funct. Mater.*, 2015, **25**, 7337.
3 X. Zou and Y. Zhang, *Chem. Soc. Rev.*, 2015, **44**, 5148.
4 (*a*) X. Zou, X. Huang, A. Goswami, R. Silva, B. R. Sathe, E. Mikmeková and T. Asefa, *Angew. Chem., Int. Ed.*, 2014, **126**, 4461; (*b*) M. S. Faber, R. Dziedzic, M. A. Lukowski, N. S. Kaiser, Q. Ding and S. Jin, *J. Am. Chem. Soc.*, 2014, **136**, 10053; (*c*) J. Tian, Q. Liu, A. M. Asiri and X. Sun, *J. Am. Chem. Soc.*, 2014, **136**, 7587; (*d*) M.-R. Gao, J.-X. Liang, Y.-R. Zheng, Y.-F. Xu, J. Jiang, Q. Gao, J. Li and S.-H. Yu, *Nat. Commun.*, 2015, **6**, 5982.
5 (*a*) C. P. Plaisance and R. A. van Santen, *J. Am. Chem. Soc.*, 2015, **137**, 14660; (*b*) G. S. Hutchings, Y. Zhang, J. Li, B. T. Yonemoto, X. Zhou, K. Zhu and F. Jiao, *J. Am. Chem. Soc.*, 2015, **137**, 4223.
6 V. Artero, M. Chavarot-Kerlidou and M. Fontecave, *Angew. Chem., Int. Ed.*, 2011, **50**, 7238.
7 (*a*) A. J. Esswein, M. J. McMurdo, P. N. Ross, A. T. Bell and T. D. Tilley, *J. Phys. Chem. C*, 2009, **113**, 15068; (*b*) J. Zhao, Y. Zou, X. Zou, T. Bai, Y. Liu, R. Gao, D. Wang and G.-D. Li, *Nanoscale*, 2014, **6**, 7255.
8 (*a*) S. Mao, Z. Wen, T. Huang, Y. Hou and J. Chen, *Energy Environ. Sci.*, 2014, **7**, 609; (*b*) M. Shen, C. Ruan, Y. Chen, C. Jiang, K. Ai and L. Lu, *ACS Appl. Mater. Interfaces*, 2015, **7**, 1207.
9 (*a*) H. Jin, J. Wang, D. Su, Z. Wei, Z. Pang and Y. Wang, *J. Am. Chem. Soc.*, 2015, **137**, 2688; (*b*) J. Li, Y. Wang, T. Zhou, H. Zhang, X. Sun, J. Tang, L. Zhang, A. M. Al-Enizi, Z. Yang and G. Zheng, *J. Am. Chem. Soc.*, 2015, **137**, 14305.
10 (*a*) H. Fei, J. Dong, M. J. Arellano-Jimenez, G. Ye, N. Dong Kim, E. L. Samuel, Z. Peng, Z. Zhu, F. Qin, J. Bao, M. J. Yacaman, P. M. Ajayan, D. Chen and J. M. Tour, *Nat. Commun.*, 2015, **6**, 8668; (*b*) Z.-Y. Wu, P. Chen, Q.-S. Wu, L.-F. Yang, Z. Pan and Q. Wang, *Nano Energy*, 2014, **8**, 118.
11 R. Liu, H. Zhang, S. Liu, X. Zhang, X. Ge, Y. Zang, H. Zhao and G. Wang, *Phys. Chem. Chem. Phys.*, 2016, **18**, 4095.
12 Y. B. Li, H. M. Zhang, Y. Wang, P. R. Liu, H. G. Yang, X. D. Yao, D. Wang, Z. Y. Tang and H. J. Zhao, *Energy Environ. Sci.*, 2014, **7**, 3720.
13 (*a*) Z. L. Wang, X. F. Hao, Z. Jiang, X. P. Sun, D. Xu, J. Wang, H. X. Zhong, F. L. Meng and X. B. Zhang, *J. Am. Chem. Soc.*, 2015, **137**, 1587; (*b*) Q. Wang, Z.-Y. Zhou, Y.-J. Lai, Y. You, J.-G. Liu, X.-L. Wu, E. Terefe, C. Chen, L. Song and M. Rauf, *J. Am. Chem. Soc.*, 2014, **136**, 10882.
14 (*a*) Z. Y. Wu, X. X. Xu, B. C. Hu, H. W. Liang, Y. Lin, L. F. Chen and S. H. Yu, *Angew. Chem., Int. Ed.*, 2015, **54**, 8179; (*b*) L. Lin, Q. Zhu and A. W. Xu, *J. Am. Chem. Soc.*, 2014, **136**, 11027.
15 (*a*) J. Wang, H. Wu, D. Gao, S. Miao, G. Wang and X. Bao, *Nano Energy*, 2015, **13**, 387; (*b*) F. Cheng and J. Chen, *Chem. Soc. Rev.*, 2012, **41**, 2172.
16 S. Cobo, J. Heidkamp, P.-A. Jacques, J. Fize, V. Fourmond, L. Guetaz, B. Jousselme, V. Ivanova, H. Dau and S. Palacin, *Nat. Mater.*, 2012, **11**, 802.
17 M. Jahan, Z. Liu and K. P. Loh, *Adv. Funct. Mater.*, 2013, **23**, 5363.